symmetry

MDPI

Article

Analysis of Magnetohydrodynamic Free Convection in Micropolar Fluids over a Permeable Shrinking Sheet with Slip Boundary Conditions

Param R. Tangsali [1], Nagaraj N. Katagi [1], Ashwini Bhat [1,*] and Manjunath Shettar [2]

[1] Department of Mathematics, Manipal Institute of Technology, Manipal Academy of Higher Education, Manipal 576104, Karnataka, India; tangsali.rudraji@learner.manipal.edu (P.R.T.)
[2] Department of Mechanical and Industrial Engineering, Manipal Institute of Technology, Manipal Academy of Higher Education, Manipal 576104, Karnataka, India
* Correspondence: ashwini.bhat@manipal.edu

Abstract: The convective micropolar fluid flow over a permeable shrinking sheet in the presence of a heat source and thermal radiation with the magnetic field directed towards the sheet has been studied in this paper. The mathematical formulation considers the partial slip condition at the sheet, allowing a realistic representation of the fluid flow near the boundary. The governing equations for the flow, heat, and mass transfer are formulated using the conservation laws of mass, momentum, angular momentum, energy, and concentration. The resulting nonlinear partial differential equations are transformed into a system of ordinary differential equations using suitable similarity transformations. The numerical solutions are obtained using robust computational techniques to examine the influence of various parameters on the velocity, temperature, and concentration profiles. The impact of slip effects, micropolar fluid characteristics, and permeability parameters on the flow features and heat transfer rates are thoroughly analyzed. The findings of this investigation offer valuable insights into the behavior of micropolar fluids in free convection flows over permeable shrinking sheets with slip, providing a foundation for potential applications in various industrial and engineering processes. Key findings include the observation that the velocity profile overshoots for assisting flow with decreasing viscous force and rising magnetic effects as opposed to opposing flow. The thermal boundary layer thickness decreases due to buoyant force but shows increasing behavior with heat source parameters. The present result agrees with the earlier findings for specific parameter values in particular cases.

Keywords: shrinking sheet; micropolar fluid; slip velocity; optimal homotopy analysis method; magnetohydrodynamic; free convection

check for updates

Citation: Tangsali, P.R.; Katagi, N.N.; Bhat, A.; Shettar, M. Analysis of Magnetohydrodynamic Free Convection in Micropolar Fluids over a Permeable Shrinking Sheet with Slip Boundary Conditions. *Symmetry* **2024**, *16*, 400. https://doi.org/10.3390/sym16040400

Academic Editor: Antonio Masiello

Received: 29 January 2024
Revised: 16 March 2024
Accepted: 22 March 2024
Published: 29 March 2024

Copyright: © 2024 by the authors. Licensee MDPI, Basel, Switzerland. This article is an open access article distributed under the terms and conditions of the Creative Commons Attribution (CC BY) license (https://creativecommons.org/licenses/by/4.0/).

1. Introduction

The study of fluid flow over surfaces, especially in the presence of heat and mass transfer, is of fundamental importance for understanding various physical phenomena and engineering applications. In this context, the investigation of magnetohydrodynamic (MHD) free convective flow of a non-Newtonian fluid over a permeable shrinking sheet, especially in the presence of heat and mass transfer, has garnered significant attention due to their prevalence in numerous industrial, biological, and environmental processes. One such intriguing scenario is the flow of a micropolar fluid over a permeable shrinking sheet. This configuration is relevant in several industrial applications, including cooling systems, materials processing, and biomedical engineering. The presence of a permeable surface introduces complexities due to the fluid–surface interaction, while the shrinking nature of the sheet adds another dimension to the problem. Moreover, incorporating slip effects at the boundary provides a more realistic representation of the fluid behavior at the interface. The interplay of micropolar

fluid characteristics, free convection, permeability, magnetic parameters, and slip affects the in-depth analysis of such systems' flow and heat transfer characteristics.

Previous studies have contributed significantly to understanding the complexities and nuances of this intricate phenomenon. The exploration of this flow scenario was initiated by Sakiadis [1–3], who investigated the flow characteristics. Subsequently, Crane [4] delved into the boundary layer flow, introducing a linear velocity profile and providing a closed-form solution. Building upon the foundational studies conducted by Sakiadis and Crane, numerous researchers in this field have undertaken investigations into different facets of boundary layer flow in Newtonian fluids ([5–10]). These subsequent studies have expanded our understanding of the behavior exhibited by fluids near stretching surfaces and have contributed valuable insights into the intricate dynamics of boundary layer flows.

The momentum and heat transfer in a power-law fluid over an unsteady stretching surface have been studied by Chen [11] and presented numerically for some values of the unsteadiness parameter and the power-law index, covering a wide range of the generalized Prandtl number. Pal and Hiremathe [12] investigated the heat transfer attributes in an incompressible viscous fluid's laminar boundary layer flow over an unsteady stretching sheet placed in a porous medium.

However, numerous engineering processes involve fluids such as lubricants, paints, blood, suspension, and colloidal fluids, which cannot be described by the classical hydrodynamics Navier–Stokes model. Early works by Eringen [13] presented the theory of micropolar fluids, emphasizing the influence of microstructure and micro-rotations within the fluid. Subsequent studies by Lukaszewicz [14] and later by Ariman et al. [15] extended the theory and elucidated the behavior of micropolar fluids in various flow scenarios. The initial model of a micropolar liquid is based on the concept of microrotation, which accounts for the additional degrees of freedom associated with the rotation of micro-elements within the fluid. This model introduces additional parameters to characterize the microstructural properties of the fluid, leading to a more comprehensive description of its behavior compared to classical Newtonian fluids. The rheological relationship for a micropolar liquid typically involves constitutive equations that incorporate both linear and angular momentum balances. These equations describe how the stress tensor and the microrotation tensor evolve in response to deformation and rotation within the fluid. A commonly used rheological relationship for micropolar fluids is the Jeffreys model, which extends the classical Newtonian model by introducing additional coefficients to characterize the microstructural effects. Ramachandran et al. thoroughly investigated the boundary layer flow of a micropolar fluid past a curved surface, exploring the impact of suction and injection on velocity, microrotation, and temperature fields [16]. Their work contributes valuable insights into the behavior of micropolar fluids, with potential applications in technology and industry.

In contrast to previous studies, Miklavčič and Wang [17] delved into the dynamics of shrinking flow, where the boundary velocity is directed towards a fixed point. This scenario differs significantly from the stretching-out case. The authors derived a closed-form solution and emphasized the necessity of mass suction to maintain the flow over a shrinking sheet. This represents a departure from conventional studies addressing flow problems associated with a shrinking sheet. Wang [18] investigated stagnation flow towards a shrinking sheet in 2008, contributing to the understanding of this specific fluid dynamics scenario. Fang [19–24] extensively explored boundary layer flow across a shrinking sheet, including the induced flow by a shrinking sheet with a power-law distribution. Fang and Zhang extended their work the analysis of heat and mass transfer over a shrinking sheet, obtaining approximate solutions and demonstrating the existence of multiple solutions to such problems.

The homotopy analysis method (HAM) is a semi-analytical technique founded by Shijun Liao. Since its inception, many variations of HAM were introduced by Liao and others. This method is used in many complex non-linear ODEs and PDEs. In 2008, Sajid et al. [25] delved into the rotating boundary layer flow of a viscous fluid induced by a shrinking

surface under the effect of the magnetic field. They used HAM to obtain solutions. Yacob and Ishak [26] analyzed a steady two-dimensional micropolar fluid flow over a shrinking sheet in its plane in 2012, contributing to the understanding micropolar fluid dynamics. In 2017, Turkyilmazoglu [27] studied MHD mixed convective flow and heat transfer due to a micropolar fluid past a heated or cooled stretching permeable surface. The study considered heat generation and absorption effects, adding complexity to fluid dynamics analysis in this specific scenario. The influence of permeability in boundary conditions has been investigated in fluid dynamics.

Convection is a recurring process involving the heating and cooling of fluid particles, where hot particles migrate to the cooler region and cold particles to the hotter region. Nield and Kuznetsov [28] presented a detailed analysis of free convection flow over permeable surfaces, emphasizing the impact of suction/injection on flow and heat transfer characteristics. Ali et al. [29], in 2011, numerically analyzed the unsteady axisymmetric flow with heat transfer and radiation effects, across a permeable shrinking sheet. They found the existence of a dual solution using the finite difference method. In 2011, Bhattacharyya and Layek [30] studied the effects of suction/blowing and thermal radiation on steady boundary layer stagnation point flow and heat transfer over a shrinking sheet. They numerically analyzed dual solutions, unique solutions, and the non-existence of solutions for self-similar flow and heat transfer equations.

According to Faraday's Law of electromagnetism, when a conducting fluid is exposed to a transverse magnetic field, the electromagnetic forces and other forces will be constituted in the equation of motion. The science dealing with these forces is known as magnetohydrodynamics (MHD). Further, in 2012, Bhattacharyya [31] analyzed the effects of thermal radiation on the flow of micropolar fluid and heat transfer past a porous shrinking sheet. The cause effects of the thermal radiation on boundary layer thickness and temperature are discussed using dual solutions. In 2016, Dash et al. [32] analyzed MHD flow, heat, and mass diffusion of electrically conducting stagnation point flow past a stretching or shrinking sheet. In 2018, Mishra et al. [33] extended the research problem explored by Bhattacharyya [31] with free convection and a heat source. The study of free convection flows, especially with non-Newtonian fluids, has been extensively explored. Bejan [34] provided a comprehensive review of natural convection phenomena, emphasizing the effects of buoyancy forces on fluid flow and heat transfer.

The slip boundary condition is one of the two main boundary conditions, the other one being the no-slip condition. Considering the slip boundary condition means assuming discontinuity of velocity function between fluid and boundary. In recent years, there has been growing recognition of the importance of slip boundary conditions in fluid flow models, particularly in the study of complex fluids. Models accounting for slip effects offer a more realistic representation of fluid flow near boundaries, contributing to enhanced accuracy in predicting flow behavior and transport phenomena. In 2014, Mansur et al. [35] studied nanofluid boundary layer flow over a stretching/shrinking sheet with velocity and thermal slip boundary conditions. They concluded that the range of the stretching/shrinking parameter increases as the velocity slip parameter increases. Baranovskii [36] investigated the optimal control problem for the stationary motion of the Jeffrey medium with the slip condition, which revealed enhanced heat transfer rates and intriguing flow features, underscoring the significance of considering slip effects in fluid dynamics studies. In the study conducted in 2019 by Dero et al. [37], the focus was on magnetohydrodynamic (MHD) micropolar nanofluid boundary layer flow over an exponentially stretching/shrinking sheet. The researchers incorporated radiation and suction effects into their analysis and applied Buongiorno's nanofluid model to the problem. Notably, their investigation resulted in a triple solution, particularly for the lower values of the magnetic parameter, thermophoresis, and material parameter, emphasizing scenarios involving high suction. Building on this work, in 2020, Bhat et al. [38] delved into the influence of slip velocity conditions at the porous disk on heat exchange. They explored the impact of the magnetic field on micropolar fluid flow between porous and non-porous

discs. Their study provided insights into the intricate interplay between slip conditions, magnetic fields, and fluid dynamics. In 2023, Guedri et al. [39] extended the scope of the problem originally presented by Dero et al. [37]. Their investigation incorporated additional complexities, including nanoparticle aggregation, MHD effects, radiation, and suction, all in the absence of a heat source. This extension aimed to broaden the understanding of the combined impact of multiple factors on nanofluid dynamics over stretching/shrinking sheets. In a separate study, Choi et al. [40] explored the significance of slip effects on the flow past a solid surface. They focused on investigating how slip conditions alter velocity and shear stress distributions. The results of their research shed light on the role of slip in modifying the boundary layer characteristics near solid surfaces, with implications for various fluid flow applications.

Despite the significant individual progress in these areas, limited attention has been paid to the combined effects of micropolar fluids, permeable shrinking surfaces, and slip conditions on free convection flows. Therefore, the present study aims to fill this gap by investigating the comprehensive interplay between these factors, providing a holistic understanding of the flow characteristics, heat transfer rates, and mass transfer in such systems. The mathematical model governing the flow, heat, and mass transfer will be formulated based on conservation laws, followed by appropriate transformations to simplify the equations for numerical analysis. Understanding the implications of this investigation holds substantial importance, as it can provide valuable insights into the behavior of micropolar fluids in practical scenarios. Additionally, the findings from this research can potentially contribute to optimizing processes in various industrial and engineering applications by offering strategies to control and manipulate fluid flow and heat transfer. This article presents a detailed analysis of the problem, encompassing the mathematical formulation, numerical methodology using the optimal homotopy method (OHAM), and discussions on the influence of pertinent parameters.

2. Materials and Methods

2.1. Mathematical Formulations

This study investigates the free convective flow of steady micropolar fluid, examining heat transfer with thermal radiation and a heat source. The research also explores the effects of magnetohydrodynamics (MHD) acting perpendicular to a permeable shrinking sheet (Figure 1).

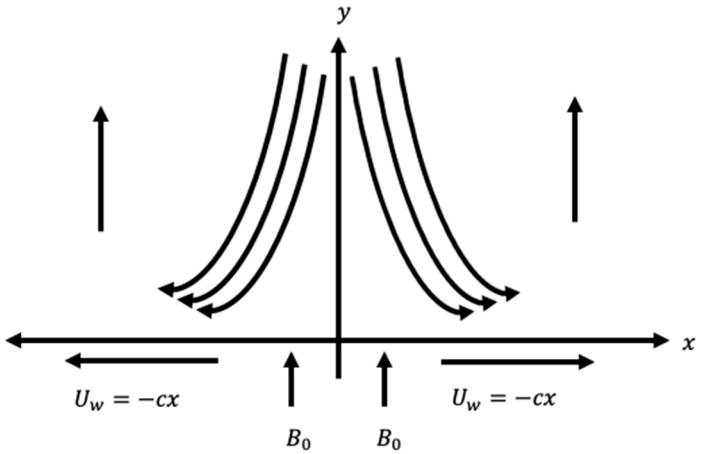

Figure 1. Geometrical model.

The velocity of the shrinking sheet is represented by $U_w = -cx$, where $c > 0$ is known as the shrinking constant. Under the boundary layer approximation, the equations governing the motion of the micropolar fluid and heat transfer, which incorporate MHD and a heat source, are as follows:

$$\frac{\partial u}{\partial x} + \frac{\partial v}{\partial y} = 0; \tag{1}$$

$$u\frac{\partial u}{\partial x}+v\frac{\partial u}{\partial y}=\left(\nu+\frac{\kappa}{\rho}\right)\frac{\partial^2 u}{\partial y^2}+\frac{\kappa}{\rho}\frac{\partial N}{\partial y}+g\beta(T-T_\infty)-\frac{\sigma_e}{\rho}B_0^2u; \tag{2}$$

$$u\frac{\partial N}{\partial x}+v\frac{\partial N}{\partial y}=\frac{\gamma}{\rho j}\frac{\partial^2 N}{\partial y^2}-\frac{\kappa}{\rho j}\left(2N+\frac{\partial u}{\partial y}\right); \tag{3}$$

$$\rho c_p\left(u\frac{\partial T}{\partial x}+v\frac{\partial T}{\partial y}\right)=\kappa*\frac{\partial^2 T}{\partial y^2}-\frac{\partial q_r}{\partial y}+Q*(T-T_\infty); \tag{4}$$

Subjected to boundary conditions,

$$\left.\begin{array}{c} u=U_w=-cx+l_1\frac{\partial u}{\partial y},\ v=v_w,\ N=-m\frac{\partial u}{\partial y},\ T=T_w\ at\ y=0 \\ u\to 0,\ N\to 0,\ T\to T_\infty\ as\ y\to\infty \end{array}\right\} \tag{5}$$

where u and v are components of velocity in the x and y direction, respectively, N is the microrotation or angular velocity normal to the xy-plane and T is the temperature. In the governing equations, ν, ρ, j, γ,κ, $\kappa*$, c_p, q_r, T_w and T_∞ represent kinematic viscosity, fluid density, microinertia per unit mass, spin gradient viscosity, vortex viscosity, the thermal conductivity of the fluid, specific heat, radiative heat flux, the temperature at the sheet and free stream temperature, respectively. In the equation, v_w is the wall mass transfer velocity where $v_w<0$ is the mass suction and $v_w>0$ is the mass injection. It is crucial to note that the constant m falls within the range of 0 to 1 for the special case where $m=0,\ N=0$ at the surface, indicating a concentrated particle flow with microelements near the wall surface unable to rotate. This situation is often referred to as an intense concentration of microelements. When $m=0.5$, it implies a weak concentration of microelements, and the anti-symmetric part of the stress tensor vanishes. On the other hand, $m=1$ is used to model turbulent boundary layer flows. The parameter l_1 represents the sheet permeability. When $l_1=0$, Equation (5) simplifies to a no-slip condition. The spin gradient viscosity (γ) is determined by

$$\gamma=\left(\mu+\frac{\kappa}{2}\right)j=\mu\left(1+\frac{K}{2}\right)j \tag{6}$$

where $K=\kappa/\mu$ represents a non-dimensional quantity known as a material parameter. This enables the system of equations to foretell the correct behaviour under the controlled scenario where microstructure effects are minimal, and the total spin N reduces to the angular velocity.

Using Rosseland's approximation for radiation, a relation for radiative heat flux can be derived as follows, i.e., $q_r=-\left(\frac{4\sigma}{3k_1}\right)\frac{\partial T^4}{\partial y}$, where σ is the Stefan–Boltzmann constant and k_1 is the absorption coefficient. Assuming a particular temperature variation within the flow, Taylor's series expansion can be applied to expand T^4. In such a scenario, expanding T^4 about T_∞ and neglecting higher-order terms one can obtain, $T^4=4T_\infty^4T-3T_\infty^4$.

Therefore, heat transfer equation can be written as

$$u\frac{\partial T}{\partial x}+v\frac{\partial T}{\partial y}=\frac{\kappa*}{\rho c_p}\frac{\partial^2 T}{\partial y^2}+\frac{16\sigma T_\infty^3}{3k_1\rho c_p}\frac{\partial^2 T}{\partial y^2}+\frac{Q*(T-T_\infty)}{\rho c_p}. \tag{7}$$

Introducing the following similarity transformation:

$$\psi=(c\nu)^{1/2}xf(\eta),\ N=cx\left(\frac{c}{\nu}\right)^{1/2}h(\eta), \tag{8}$$

$$T=T_\infty+(T_w-T_\infty)\theta(\eta)\text{ and }\eta=\left(\frac{c}{\nu}\right)^{1/2}y, \tag{9}$$

where ψ is the stream function. The continuity equation is fulfilled, and Equations (2), (3) and (7) are reduced using the above similarity transformation to the following nonlinear ordinary differential equations:

$$(1+K)f'''+ff''-f'^2+Kh'+Gr\,\theta-Ma\,f'=0, \tag{10}$$

$$(1+K/2)h'' + fh' - f'h - K(2h+f'') = 0, \tag{11}$$

$$(3R+4)\theta'' + 3PrRf\theta' + 3PrR\lambda\theta = 0, \tag{12}$$

where the non-dimensional quantities $Pr = \frac{\mu c_p}{\kappa*}$, $R = \frac{\kappa* k_1}{4\sigma T_\infty^3}$, $Gr = \frac{g\beta(T_w - T_\infty)}{-cU_w}$, $\lambda = \frac{Q*}{c(\rho c_p)}$, $Ma = \frac{\sigma_e}{\rho c} B_0^2$ represent the Prandtl number, thermal radiation parameter, free convective parameter or Grashof number, heat source parameter and magnetic parameter.

The transformed conditions are

$$f(\eta) = S,\ f'(\eta) = -1 + \phi f''(\eta)\ ,\ h(\eta) = -mf''(\eta),\ \theta(\eta) = 1\ at\ \eta = 0, \tag{13}$$

$$f'(\eta) \to 0,\ h(\eta) \to 0,\ \theta(\eta) \to 0\ at\ \eta \to \infty \tag{14}$$

where $S = -\frac{v_w}{(c\nu)^{1/2}}$ depicts wall mass transfer. $S > 0$ corresponds to mass suction and $S < 0$ corresponds to mass injection. $\phi = l_1 \left(\frac{c}{\nu}\right)^{1/2}$ is the slip coefficient. When $\phi = 0$, the boundary condition of the problem reduces to a no-slip condition.

2.2. Methodology

The Equations (10)–(12) subjected to boundary conditions (13) and (14) are solved using the OHAM. The theory of the homotopy analysis method (HAM) was introduced by Shijun Liao [41] and was extended to many forms. The auxiliary linear operator and initial guess are chosen as

$$L_1[u] = u''' - u',\ L_2[u] = u'' - u,\ L_3[u] = u'' - u \tag{15}$$

$$f_0 = \frac{e^{-\eta} - 1}{1+\phi} + S,\ h_0 = -m\frac{e^{-\eta}}{1+\phi},\ \theta_0 = e^{-\eta} \tag{16}$$

The auxiliary functions are chosen as $H[\eta, i] = e^{-\eta}$ for $i = 1, 2, 3$; where the i values specifically represent the velocity, microrotation, and temperature profiles, respectively. All three auxiliary linear operators will satisfy $L_1[C_1 + C_2 e^{-\eta} + C_3 e^{\eta}] = 0$; $L_j[C_4 e^{-\eta} + C_5 e^{\eta}] = 0$, $j = 2, 3$; where C_i's $(i = 1, 2, 3, 4, 5)$ are arbitrary constants.

2.3. Zeroth-Order Deformation Problems

$$(1-q)L_1\left[\widetilde{f}(\eta, q) - f_0(\eta)\right] = q\hbar H[\eta, 1]N_1\left[\widetilde{f}, \widetilde{h}, \widetilde{\theta}\right], \tag{17}$$

$$(1-q)L_2\left[\widetilde{h}(\eta, q) - h_0(\eta)\right] = q\hbar H[\eta, 2]N_2\left[\widetilde{f}, \widetilde{h}, \widetilde{\theta}\right], \tag{18}$$

$$(1-q)L_3\left[\widetilde{\theta}(\eta, q) - \theta_0(\eta)\right] = q\hbar H[\eta, 3]N_3\left[\widetilde{f}, \widetilde{h}, \widetilde{\theta}\right] \tag{19}$$

$$\begin{gathered}\widetilde{f}(0,q) = S, \widetilde{f}'(0,q) = -1 + \widetilde{f}''(0,q), \widetilde{h}(0,q) = -m\widetilde{f}''(0,q), \widetilde{\theta}(0,q) = 1 \\ \widetilde{f}'(\infty, q) = 0,\ \widetilde{h}(\infty, q) = 0,\ \widetilde{\theta}(\infty, q) = 0\end{gathered} \tag{20}$$

where $q \in [0, 1]$ is the embedding parameter, $\hbar$ is the control convergence parameter, $N_i,\ i = 1, 2, 3$ are nonlinear operators for f, h, θ, respectively, in which Equations (10)–(12) will be written as a function of η and q.

For $q = 0$ and $q = 1$, we have

$$\begin{gathered}\widetilde{f}(\eta, 0) = f_0(\eta),\ \widetilde{h}(\eta, 0) = h_0(\eta),\ \widetilde{\theta}(\eta, 0) = \theta_0(\eta), \\ \widetilde{f}(\eta, 1) = f(\eta),\ \widetilde{h}(\eta, 1) = h(\eta),\ \widetilde{\theta}(\eta, 1) = \theta(\eta).\end{gathered} \tag{21}$$

As q increases from 0 to 1, $\widetilde{f}$, $\widetilde{h}$, $\widetilde{\theta}$ varies from initial guesses f_0, h_0, θ_0 to exact solutions f, h, θ. According to Taylor's theorem,

$$f(\eta,q) = f_0(\eta) + \sum_{m=1}^{\infty} f_m(\eta)q^m,\ h(\eta,q) = h_0(\eta) + \sum_{m=1}^{\infty} h_m(\eta)q^m,$$
$$\theta(\eta,q) = \theta_0(\eta) + \sum_{m=1}^{\infty} \theta_m(\eta)q^m \tag{22}$$

where

$$f_m(\eta) = \frac{1}{m!}\frac{\partial^m \widetilde{f}(\eta,q)}{\partial\, q^m}\bigg|_{q=0}, h_m(\eta) = \frac{1}{m!}\frac{\partial^m \widetilde{h}(\eta,q)}{\partial\, q^m}\bigg|_{q=0}, \theta_m(\eta) = \frac{1}{m!}\frac{\partial^m \widetilde{\theta}(\eta,q)}{\partial\, q^m}\bigg|_{q=0}$$

2.4. m^{th}-Order Deformation Problem

The mth-order deformation problems for f, h, θ are given by

$$L_1[f_m(\eta) - \chi_m f_{m-1}(\eta)] = \hbar H[\eta,1]R_m^f(\eta), \tag{23}$$

$$L_1[h_m(\eta) - \chi_m h_{m-1}(\eta)] = \hbar H[\eta,2]R_m^h(\eta), \tag{24}$$

$$L_1[\theta_m(\eta) - \chi_m \theta_{m-1}(\eta)] = \hbar H[\eta,3]R_m^\theta(\eta), \tag{25}$$

subject to boundary conditions

$$f_m(0) = 0,\ f_m'(0) = 0,\ h_m(0) = 0, \theta_m(0) = 0,\ f_m(\infty) = 0,\ h_m(\infty) = 0,\ \theta_m(\infty) = 0. \tag{26}$$

where

$$R_m^f(\eta) = \frac{1}{(m-1)!}\frac{\partial^{m-1}N[f(\eta,q)]}{\partial q^{m-1}}\bigg|_{q=0} = \frac{1}{(m-1)!}\left(\frac{\partial^{m-1}}{\partial q^{m-1}}N\left[\sum_{m=0}^{\infty} f_m(\eta)q^m\right]\right)\bigg|_{q=0}$$

$$R_m^h(\eta) = \frac{1}{(m-1)!}\frac{\partial^{m-1}N[h(\eta,q)]}{\partial q^{m-1}}\bigg|_{q=0} = \frac{1}{(m-1)!}\left(\frac{\partial^{m-1}}{\partial q^{m-1}}N\left[\sum_{m=0}^{\infty} h_m(\eta)q^m\right]\right)\bigg|_{q=0}$$

$$R_m^\theta(\eta) = \frac{1}{(m-1)!}\frac{\partial^{m-1}N[\theta(\eta,q)]}{\partial q^{m-1}}\bigg|_{q=0} = \frac{1}{(m-1)!}\left(\frac{\partial^{m-1}}{\partial q^{m-1}}N\left[\sum_{m=0}^{\infty} \theta_m(\eta)q^m\right]\right)\bigg|_{q=0}$$

and $\chi_m = \begin{cases} 0, & m \le 1 \\ 1, & m > 1 \end{cases}$.

MATHEMATICA 13.2 combined with Wolfram Cloud has been used to solve the system of governing equations using OHAM for a fast runtime.

3. Results

By presenting and discussing the results obtained by solving the coupled nonlinear ordinary differential Equations (10)–(12) using the semi-analytical technique OHAM in the context of existing literature and theoretical implications, this section would provide a comprehensive understanding of the interplay between slip effects, micropolar fluid dynamics, permeable surfaces, and their implications for heat and mass transfer in this flow configuration.

Figure 2 represents the velocity profile, microrotation profile, and temperature profile for various material parameter K and magnetic parameter Ma with given pertinent parameters. Figure 2a shows that velocity profiles are increasing with an increase in magnetic parameters. This can be attributed to strengthening the magnetic field's influence on the fluid flow, including the generation of Lorentz forces, suppression of convection currents, enhanced shear stress, and thinning of the magnetic boundary layer. But it lowers itself

with material parameter K. This is due to increased internal damping, enhanced viscosities, the influence of micro-inertia effects, alterations in flow patterns, and the generation of microscale vorticity. These microstructural effects collectively contribute to the overall reduction in fluid motion as the material parameter increases. In Figure 2b, we see that the microrotation profile shows decreasing behavior near the shrinking sheet for magnetic parameter Ma. This is a result of the combined effects of the Lorentz force resisting microrotation, the magnetic field's suppression of microrotational effects, the thinning of the boundary layer, and the dominance of the magnetic field over the micropolar fluid's microstructure near the surface. Additionally, due to the permeability or porosity of the shrinking sheet, the microrotation profile increases with increasing material parameter K. In Figure 2c, the decrease in temperature profiles with an increase in the magnetic parameter Ma over the shrinking sheet is primarily attributed to the work carried out by the Lorentz force, which opposes the fluid motion induced by temperature gradients. This suppression of convective heat transfer, coupled with enhanced heat dissipation and potential cooling effects, reduces the fluid temperature. The increase in temperature profiles with an increase in the material parameter K can be attributed to the intricate interplay of microstructural features in the micropolar fluid, including enhanced microscopic heat transfer, micro-rotation-induced mixing, increased dissipation, improved thermal conduction, and the formation of microscale vortical structures. These factors collectively contribute to a more efficient heat transfer within the fluid, resulting in higher temperature profiles as the material parameter increases.

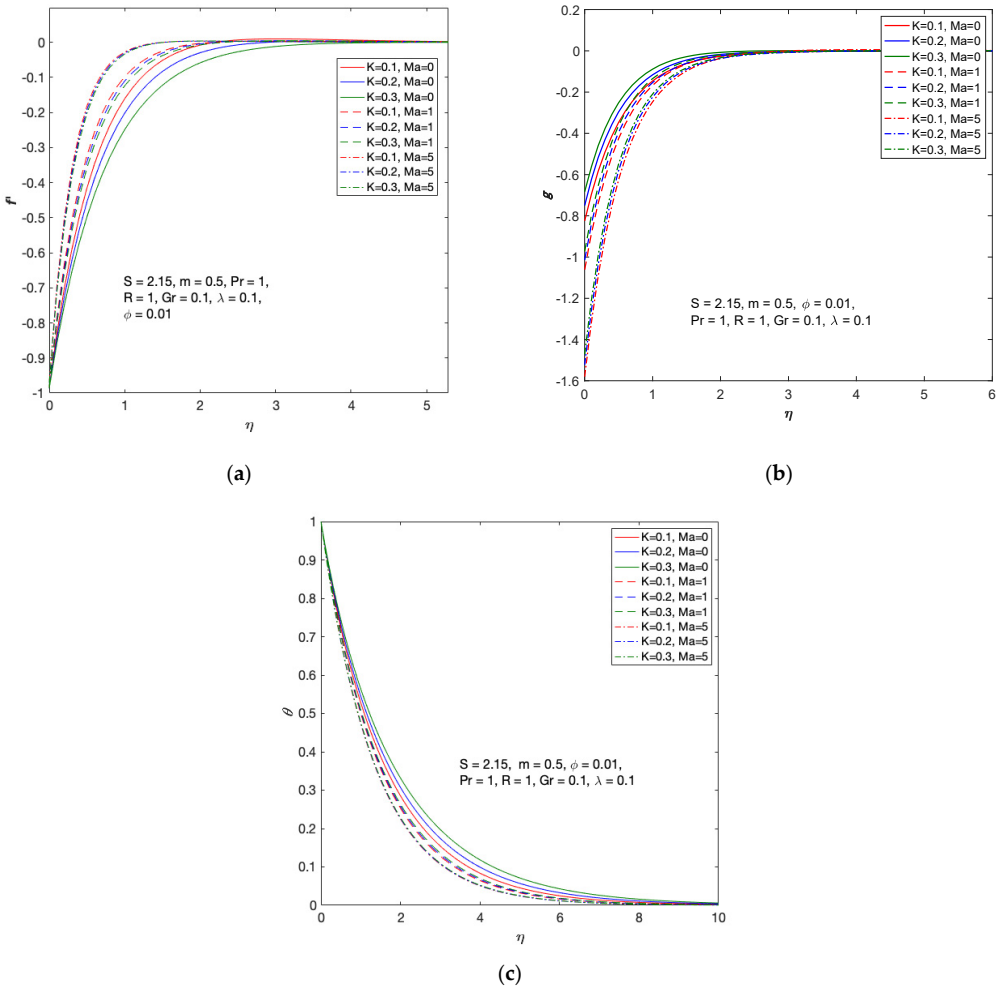

Figure 2. Variation in (**a**) velocity profile, (**b**) microrotation profile and (**c**) temperature profile for K with Ma using $S = 2.15,\ m = 0.5,\ \phi = 0.01,\ Pr = 1,\ R = 1,\ Gr = 0.1,\ \lambda = 0.14$.

Figure 3 shows the velocity profile, microrotation profile and temperature profile for material parameter K and slip coefficient ϕ with given pertinent parameters. In the above figures, velocity, microrotation, and temperature profiles show the same behaviour for material parameter K as in Figure 2. In Figure 3a, b, the velocity profile and microrotation profile, respectively, flatten near the shrinking sheet as the slip coefficient ϕ increases. The slip condition alters the fluid–solid interaction, leading to more uniform and smoother fluid motion near the surface. As the slip coefficient ϕ increases, the physical effects include enhanced shear stress, changes in velocity profiles, reduced frictional resistance, increased shear rate, thinning of the velocity boundary layer, and greater momentum transfer. These factors collectively contribute to an increase in the thickness of the boundary layer. In Figure 3c, the thermal boundary layer thickness decreases with increasing slip velocity.

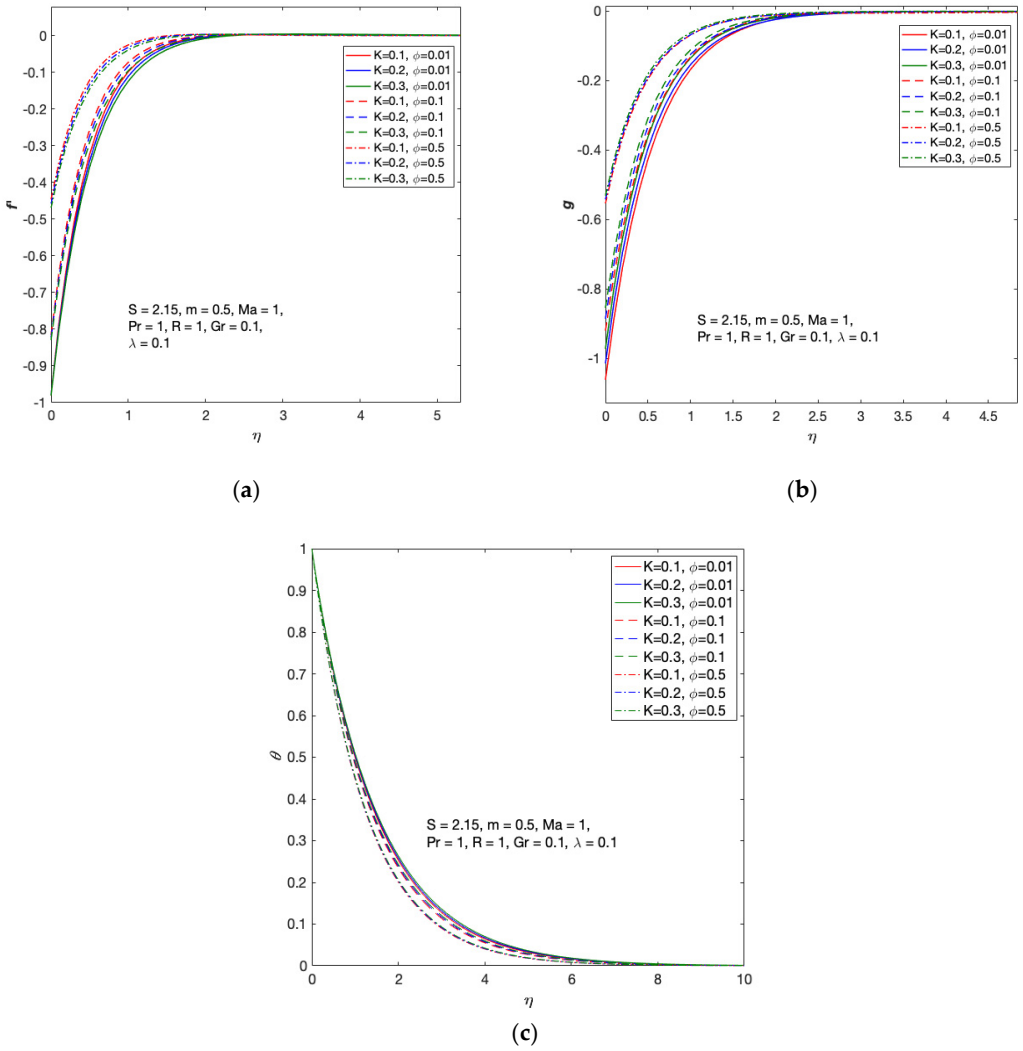

Figure 3. Variation in (**a**) velocity profile, (**b**) microrotation profile and (**c**) temperature profile for K and ϕ with $S = 2.15,\ m = 0.5,\ Ma = 1,\ Pr = 1,\ R = 1,\ Gr = 0.1,\ \lambda = 0.1$.

In Figure 4, a graphical representation of the velocity profile, microrotation profile and temperature profile is shown for different magnetic parameter Ma and slip coefficient ϕ. It is observed that Lorentz force is independent of the effect of the slip coefficient on all the profiles as both the magnetic parameter and slip coefficient show the same trend of behaviors for different values. Lorentz force operates independently of the slip coefficient, influencing the fluid–solid interface's relative motion.

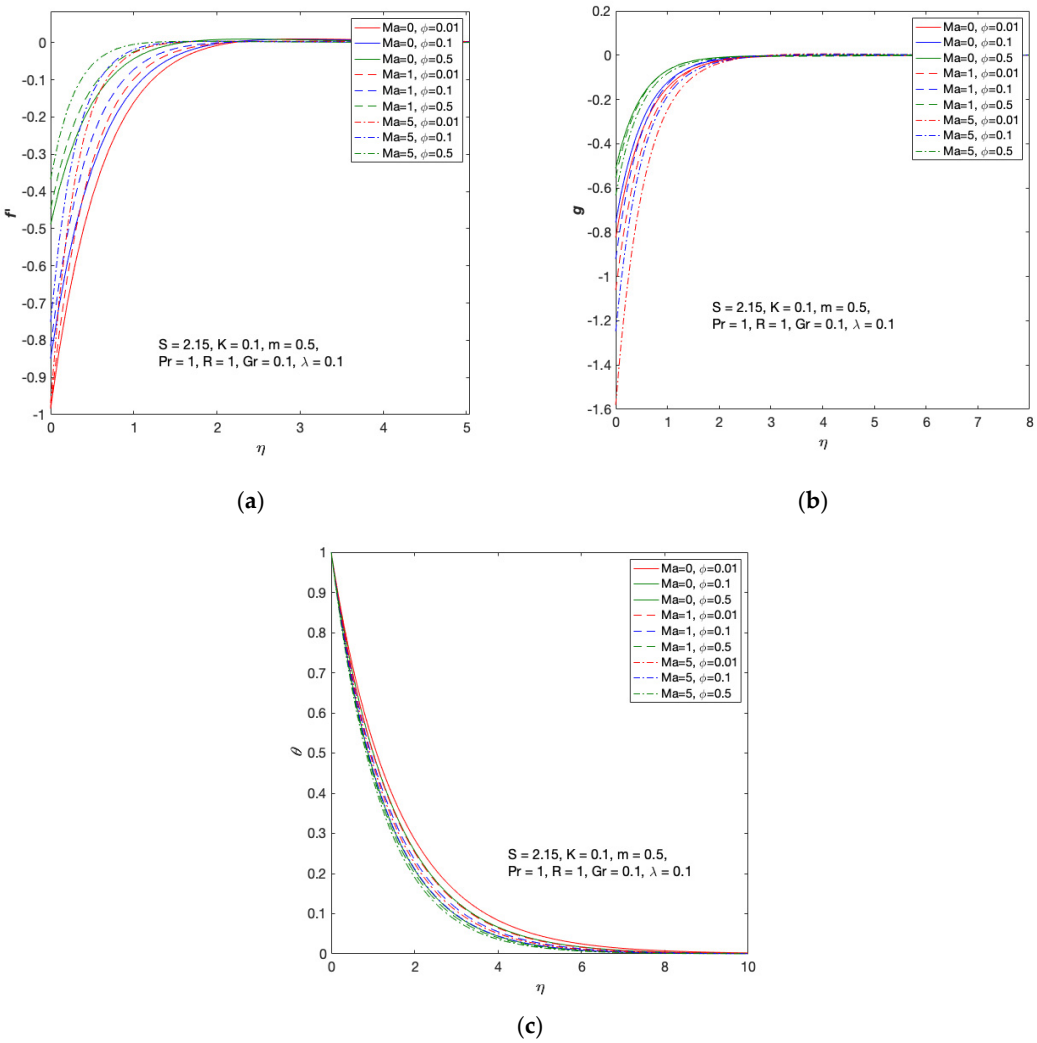

Figure 4. Variation in (**a**) velocity profile, (**b**) microrotation profile and (**c**) temperature profile for Ma and ϕ with $S = 2.15,\ K = 0.1,\ m = 0.5,\ Pr = 1,\ R = 1,\ Gr = 0.1,\ \lambda = 0.1$.

Figure 5 shows the velocity profile, microrotation profile, and temperature profile for various suction mass transfer S and magnetic parameter Ma with given pertinent parameters. In Figure 5a, the velocity profile rises with increasing suction mass transfer S near the shrinking sheet. Hence, the boundary layer also increases with S. In Figure 5b, the microrotation profile decreases near the shrinking sheet with increasing suction parameter S, and then it starts increasing with S as it goes to zero. Initially, suction dominates, leading to a reduction in microrotation. As S increases further, shear forces become significant, causing transitional behavior in the microrotation profile. For higher suction parameter S, the microrotation profile decreases near the shrinking sheet and then starts increasing for the increasing magnetic parameter as it goes to zero. In Figure 5c, the temperature profile decreases for the suction parameter S and the magnetic parameter Ma.

Figure 6 shows the velocity profile and microrotation profile for various constant m and magnetic parameter Ma with given pertinent parameters. Both velocity and microrotation profiles show the same behaviour for magnetic parameter due to Lorentz force. In Figure 6a, as the constant m increases, the velocity profile increases near the shrinking sheet. In Figure 6b, the microrotation profile at and near the shrinking sheet decreases with increasing constant m.

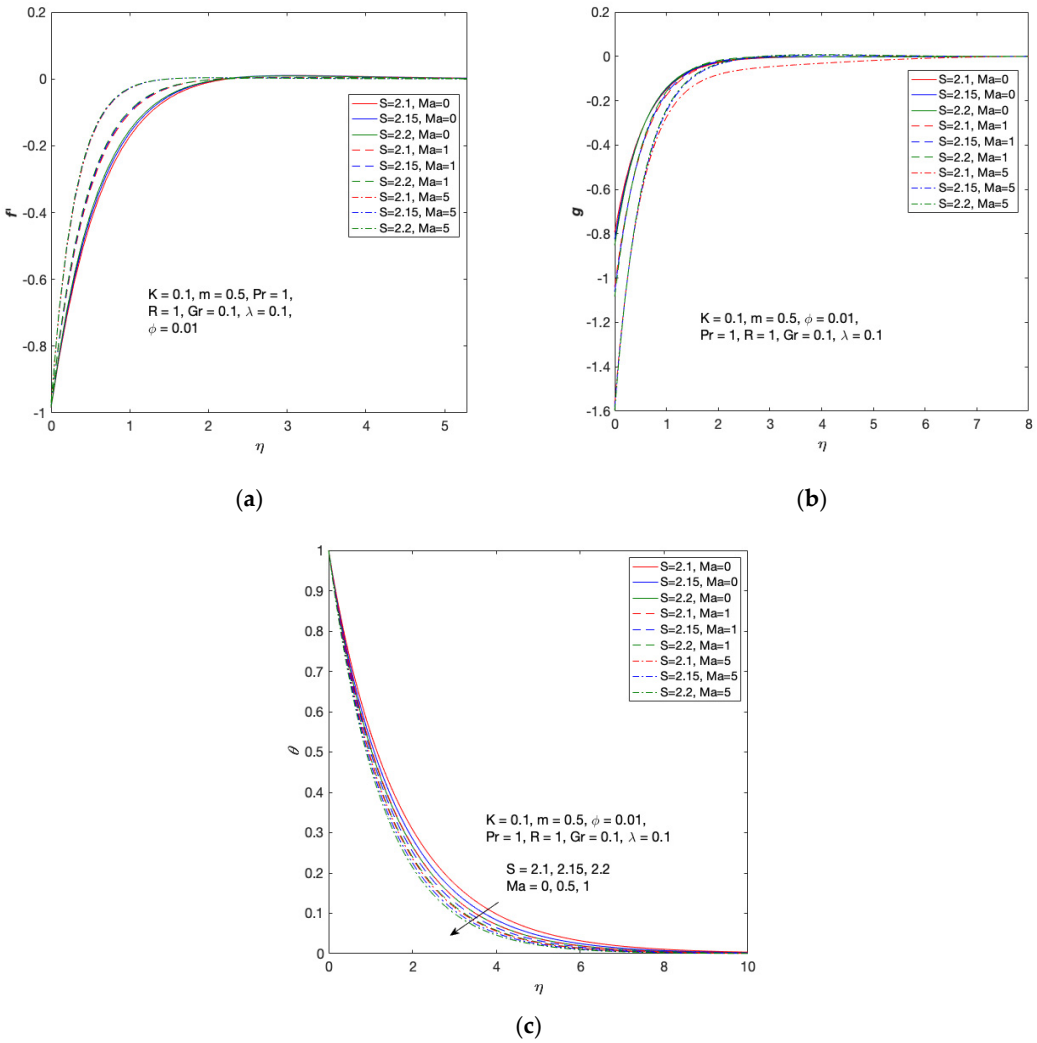

Figure 5. Variation in (**a**) velocity profile, (**b**) microrotation profile and (**c**) temperature profile for S with Ma using $K = 0.1,\ m = 0.5,\ \phi = 0.01,\ Pr = 1,\ R = 1,\ Gr = 0.1,\ \lambda = 0.1$.

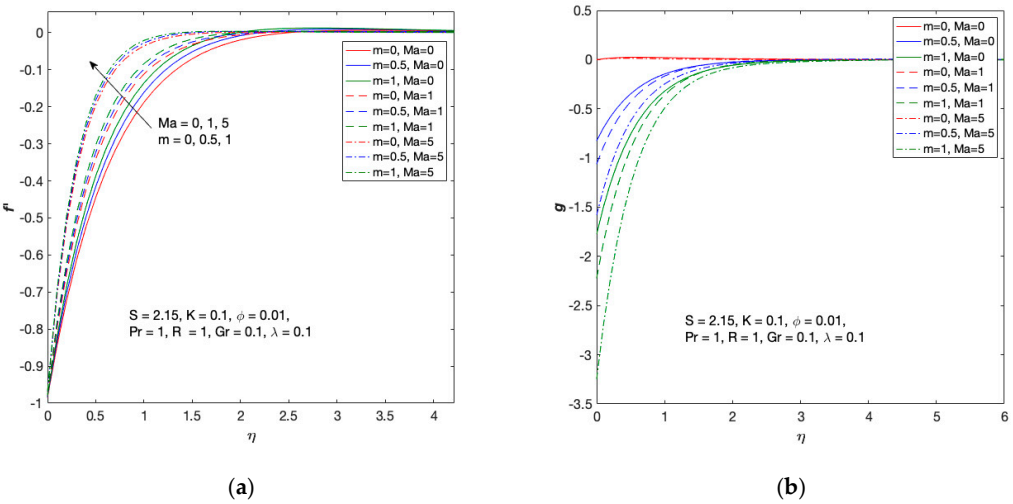

Figure 6. Variation in (**a**) velocity profile and (**b**) microrotation profile for m with Ma using $S = 2.15,\ K = 0.1,\ \phi = 0.01,\ Pr = 1,\ R = 1,\ Gr = 0.1,\ \lambda = 0.1$.

Figure 7 shows the temperature profile for various Prandtl number Pr and thermal radiation parameters R with a variation in the magnetic parameter and other values of pertinent parameters. The temperature profile shows decreasing behavior for both the Prandtl number Pr and thermal radiation parameter R in both figures as it asymptotically goes to zero.

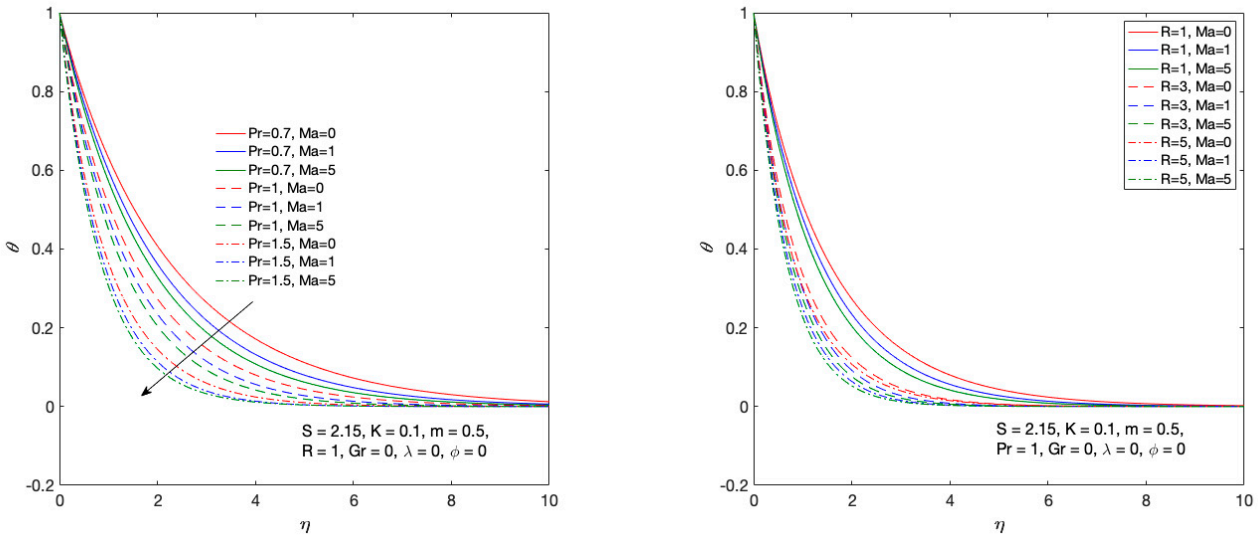

(**a**) (**b**)

Figure 7. Variation in temperature profile for (**a**) Pr, (**b**) R with Ma using $S = 2.15$, $K = 0.1$, $m = 0.5$, $\phi = 0$, $\lambda = 0.1$.

Figure 8 displays the velocity profile for various negative values of free convective parameter Gr and the magnetic parameter with and without heat source parameter λ**.** In Figure 8a, due to buoyancy force, the velocity profile near the shrinking sheet increases with an increasing Grashof number Gr. The buoyancy force also increases the boundary layer thickness with increasing Gr. In Figure 8b, the velocity profile shows the same behavior as Figure 8a. The velocity profile increases with an increasing heat source parameter λ.

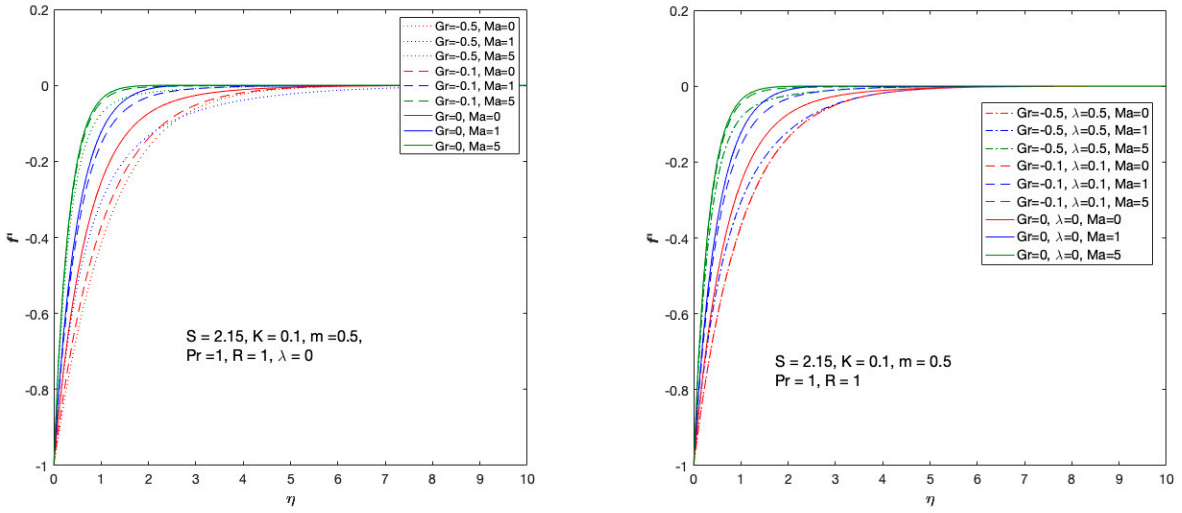

(**a**) (**b**)

Figure 8. Variation in velocity profile for negative Gr (**a**) without λ and (**b**) λ with Ma using $S = 2.15, K = 0.1, m = 0.5, \phi = 0.01, Pr = 1, R = 1$.

Figure 9 depicts the velocity profile for various positive values of free convective parameter Gr and magnetic parameter Ma with and without heat source parameter λ. In both figures, the velocity profile increases for the increasing Grashof number and heat source parameter λ, and it overshoots near the shrinking sheet, going against the shrinking sheet velocity for higher Gr $(Gr \geq 0.1)$. As a consequence of Lorentz force, after overshooting, the velocity profile decreases with an increasing magnetic parameter near the shrinking sheet as it converges to zero.

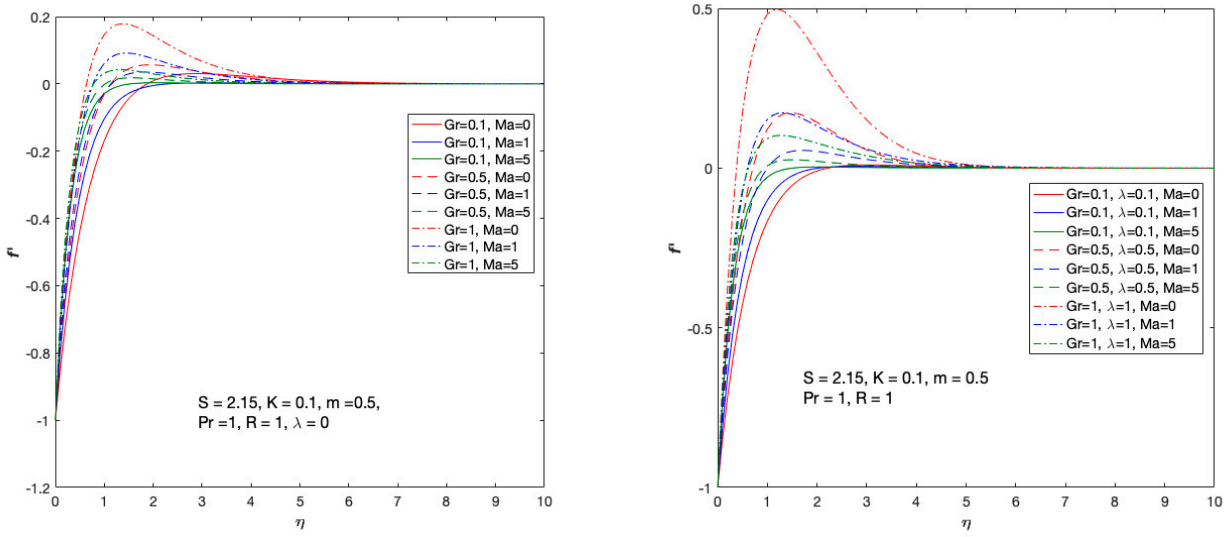

(**a**) (**b**)

Figure 9. Variation in velocity profile for positive Gr (**a**) without λ and (**b**) λ with Ma using $S = 2.15$, $K = 0.1$, $m = 0.5$, $\phi = 0.01$, $Pr = 1$, $R = 1$.

Figure 10 depicts the microrotation profile for various negative values of free convective parameter Gr and magnetic parameter Ma with and without heat source parameter λ. Due to buoyancy, the microrotation profile decreases with an increasing Grashof number. With a negative Grashof number, increasing the heat source parameter increases the microrotation profile.

Figure 11 depicts the microrotation profile for various positive values of free convective parameter Gr and magnetic parameter Ma with and without heat source parameter λ. In both figures, the microrotation profile decreases with an increasing Grashof number near the shrinking sheet. With an increasing Grashof number, the microrotation profile increases away from the shrinking sheet, but the presence of a heat source parameter minimizes this.

Figure 12 shows temperature profiles for free convective parameter Gr and magnetic parameter Ma with and without heat source parameter λ. In Figure 12a, it can be observed that the thermal boundary layer decreases initially as the Grashof number increases from a negative value. However, as the Grashof number reaches a positive value, the trend shifts to an increasing profile with Gr. This change in trend is due to the buoyancy force, as the free convective parameter Gr shifts from negative to positive value. Similarly, in Figure 12b, we can see that the temperature profile increases as the Grashof number and heat source parameter increase due to the buoyancy effect. However, the thermal boundary layer decreases with an increasing magnetic parameter Ma, as a consequence of Lorentz force.

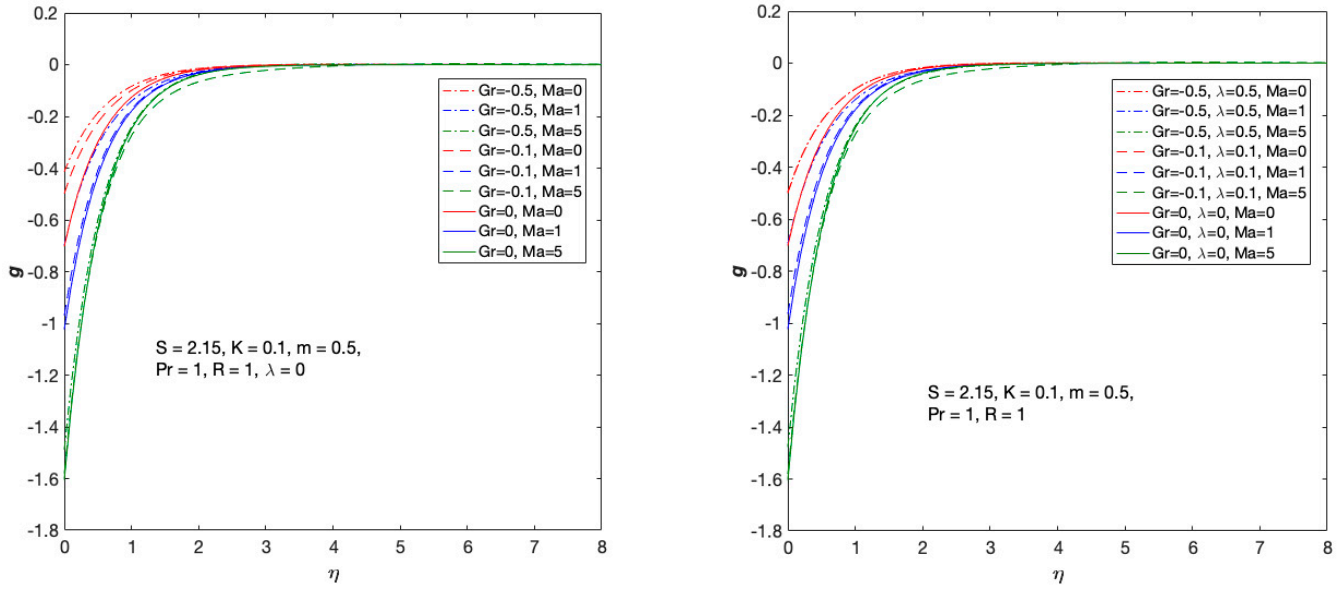

(**a**) (**b**)

Figure 10. Variation in microrotation profile for negative Gr (**a**) without λ and (**b**) λ with Ma using $S = 2.15,\ K = 0.1,\ m = 0.5,\ \phi = 0.01,\ Pr = 1,\ R = 1$.

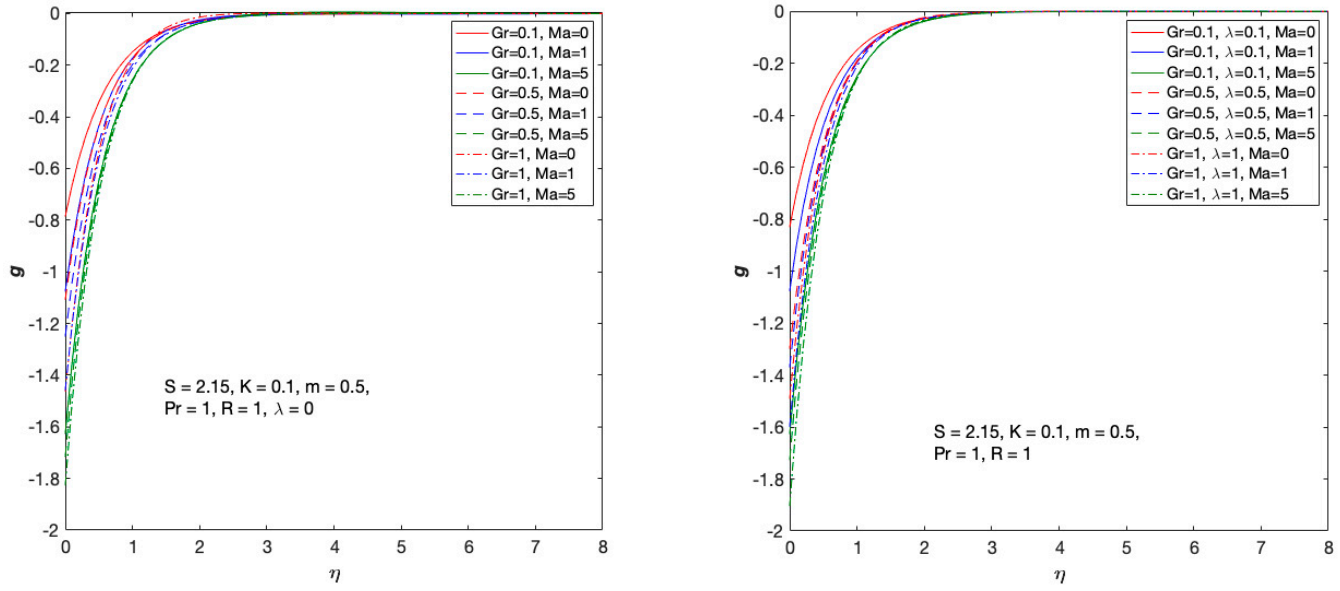

(**a**) (**b**)

Figure 11. Variation in microrotation profile for positive Gr (**a**) without λ and (**b**) λ with Ma using $S = 2.15,\ K = 0.1,\ m = 0.5,\ \phi = 0.01,\ Pr = 1,\ R = 1$.

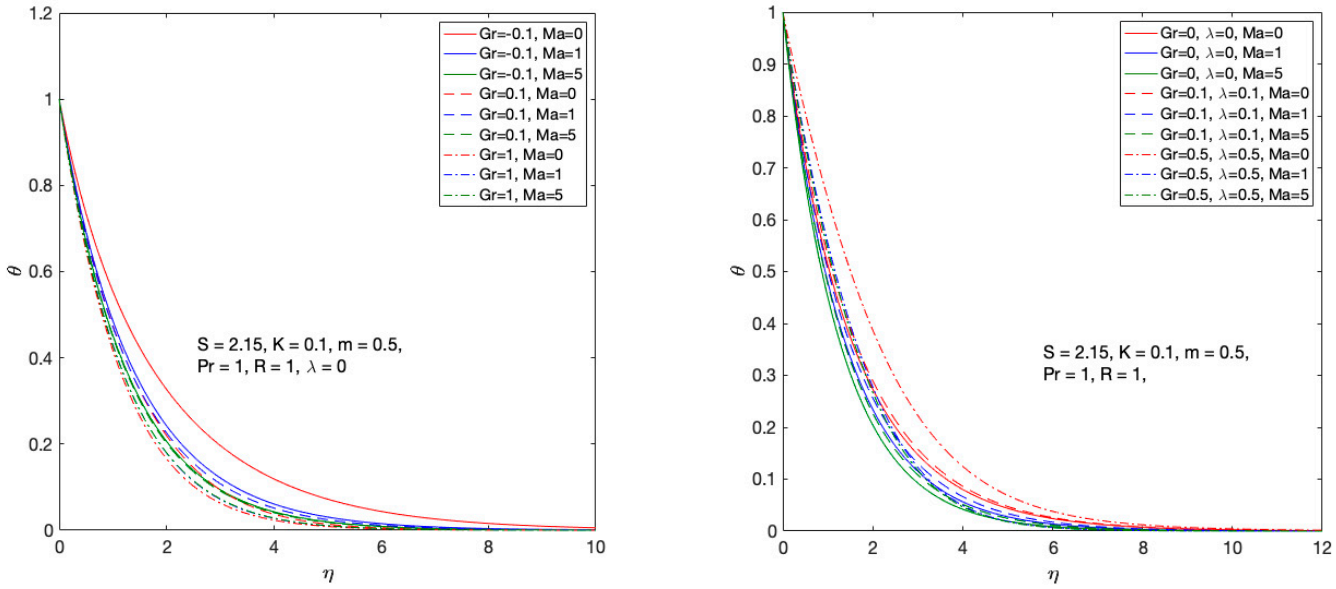

(**a**) (**b**)

Figure 12. Variation in temperature profile for Gr (**a**) without λ and (**b**) λ with Ma using $S = 2.15$, $K = 0.1$, $m = 0.5$, $\phi = 0.01$, $Pr = 1$, $R = 1$.

4. Conclusions

In this study, we investigated the free convection flow of a micropolar fluid over a permeable shrinking sheet, accounting for slip effects at the boundary. This research problem is successfully solved using OHAM. The numerical analysis and discussions presented shed light on the intricate interplay between various factors influencing flow characteristics, heat transfer rates, and mass transport in such systems.

Key findings from this investigation include the following:

- Incorporating slip conditions at the boundary significantly affects the flow behavior near the surface. The altered velocity profiles and shear stress distributions due to slip have notable implications for boundary layer development and heat transfer rates.
- The study underscores the significant impact of magnetic fields and micropolar fluid characteristics on flow patterns, heat transfer, and microrotation effects. The interplay of these factors governs the system's overall behavior, influencing boundary layer development and flow structures.
- The micropolar fluid properties, particularly the microinertia density and material constants, are crucial in shaping the flow patterns, micro-rotational effects, and thermal characteristics. These parameters influence the fluid's response to the shrinking sheet and permeability effects.
- Efforts have been made to validate theoretical findings by comparing them with the available literature to ensure the accuracy and reliability of the proposed model and the numerical solutions obtained. The present solutions agree with the first solution given in [31] by Bhattacharyya et al.

The comprehensive analysis presented in this study contributes to understanding micropolar fluid dynamics in complex flow scenarios. The findings have direct implications for industrial applications such as coating processes, materials manufacturing, and heat exchanger design. Understanding the complex fluid dynamics and heat transfer behavior is essential for optimizing these processes and enhancing efficiency.

The limitation of the current study is that the numerical approach employed, while robust, may have computational limitations in handling extremely complex geometries or boundary conditions. In this regard, further investigation could focus on extending the

study to more complex geometries or configurations under turbulent conditions relevant to practical engineering applications.

Author Contributions: Conceptualization, P.R.T. and A.B.; methodology, P.R.T. and A.B.; software, P.R.T.; validation, P.R.T., N.N.K. and A.B.; formal analysis, P.R.T., N.N.K., A.B. and M.S.; writing—original draft preparation, P.R.T. and A.B.; writing—review and editing, N.N.K. and M.S.; supervision, N.N.K. and M.S.; project administration, N.N.K. All authors have read and agreed to the published version of the manuscript.

Funding: This research received no external funding.

Data Availability Statement: The data that support the findings of this study are available from the corresponding author [A.B.], upon reasonable request.

Conflicts of Interest: The authors declare no conflicts of interest.

Nomenclature

(x, y, z) Cartesian coordinates	g gravity
B_0 Magnetic field component	(f, h, θ) Dimensionless function
T Temperature	ν Dynamic viscosity
T_w Temperature at the sheet	T_∞ free stream temperature
j Micro inertia	c Shrinking constant
Ma magnetic parameter	ρ Density
κ Vortex viscosity	$u = (u, v)$ Velocity vector
N Microrotation or angular velocity	γ Spin gradient viscosity
$\kappa*$ Thermal conductivity	μ Coefficient of viscosity
v_w Wall mass transfer	σ_e Conductivity of the medium
m Constant	l_1 Sheet permeability
K Material parameter	q_r Radiative heat flux
k_1 Absorption coefficient	$Q*$ Source/sink coefficient
σ Stefan–Boltzmann constant	c_p Specific heat
Pr Prandtl number	R Radiation parameter
Gr Grashof number	λ Heat source parameter
ψ Stream function	η Non-dimensional length or variable
S Wall mass transfer parameter	ϕ Slip coefficient
$L_i,\ i = 1, 2, 3$ Linear operator	$f_0,\ h_0,\ \theta_0$ Initial guess for OHAM
$H[\eta, i],\ i = 1, 2, 3$ Auxiliary function	q Embedding parameter
$\hbar$ Control convergence parameter	$N_i,\ i = 1, 2, 3$ Non- linear operator

References

1. Sakiadis, B.C. Boundary-layer behavior on continuous solid surfaces: I. Boundary-layer equations for two-dimensional and axisymmetric flow. *AIChE J.* **1961**, *7*, 26–28. [CrossRef]
2. Sakiadis, B.C. Boundary-layer behavior on continuous solid surfaces: II. The boundary layer on a continuous flat surface. *AiChE J.* **1961**, *7*, 221–225. [CrossRef]
3. Sakiadis, B.C. Boundary-layer behavior on continuous solid surfaces: III. The boundary layer on a continuous cylindrical surface. *AiChE J.* **1961**, *7*, 467–472. [CrossRef]
4. Crane, L.J. Flow past a stretching plate. *Z. Für Angew. Math. Und Phys. ZAMP* **1970**, *21*, 645–647. [CrossRef]
5. Afzal, N. Momentum transfer on power law stretching plate with free stream pressure gradient. *Int. J. Eng. Sci.* **2003**, *41*, 1197–1207. [CrossRef]
6. Fang, T. Similarity solutions for a moving-flat plate thermal boundary layer. *Acta Mech.* **2003**, *163*, 161–172. [CrossRef]
7. Fang, T.; Zhang, J.; Yao, S. Slip MHD viscous flow over a stretching sheet—An exact solution. *Commun. Nonlinear Sci. Numer. Simul.* **2009**, *14*, 3731–3737. [CrossRef]
8. Fang, T.; Jing, W. Flow, heat, and species transfer over a stretching plate considering coupled Stefan blowing effects from species transfer. *Commun. Nonlinear Sci. Numer. Simul.* **2014**, *19*, 3086–3097. [CrossRef]
9. Kudenatti, R.B.; Kirsur, S.R.; Achala, L.N.; Bujurke, N.M. MHD boundary layer flow over a nonlinear stretching boundary with suction and injection. *Int. J. Non-Linear Mech.* **2013**, *50*, 58–67. [CrossRef]
10. Wang, C.Y. Analysis of viscous flow due to a stretching sheet with surface slip and suction. *Nonlinear Anal. Real World Appl.* **2009**, *10*, 375–380. [CrossRef]

11. Chen, C.-H. Heat transfer in a power-law fluid film over a unsteady stretching sheet. *Heat Mass Transf.* **2003**, *39*, 791–796. [CrossRef]
12. Pal, D.; Hiremath, P.S. Computational modeling of heat transfer over an unsteady stretching surface embedded in a porous medium. *Meccanica* **2010**, *45*, 415–424. [CrossRef]
13. ERINGEN, A.C. Theory of Micropolar Fluids. *J. Math. Mech.* **1966**, *16*, 1–18. Available online: http://www.jstor.org/stable/24901466 (accessed on 28 January 2024). [CrossRef]
14. Turk, T.A.M.A.; Sylvester, N.D. Application of microcontinum fluid mechanics. *Int. J. Eng. Sci.* **1974**, *12*, 273–293.
15. Lukaszewicz, G. *Micropolar Fluids: Theory and Applications*; Modeling and Simulation in Science, Engineering and Technology; Birkhäuser: Basel, Switzerland, 1999.
16. Ramachandran, P.S.; Mathur, M.N.; Ojha, S.K. Heat transfer in boundary layer flow of a micropolar fluid past a curved surface with suction and injection. *Int. J. Eng. Sci.* **1979**, *17*, 625–639. [CrossRef]
17. Miklavčič, M.; Wang, C.Y. Viscous flow due to a shrinking sheet. *Q. Appl. Math.* **2006**, *64*, 283–290. [CrossRef]
18. Wang, C.Y. Stagnation flow towards a shrinking sheet. *Int. J. Nonlinear Mech.* **2008**, *43*, 377–382. [CrossRef]
19. Fang, T. Boundary layer flow over a shrinking sheet with power-law velocity. *Int. J. Heat Mass Transf.* **2008**, *51*, 5838–5843. [CrossRef]
20. Fang, T.; Liang, W.; Lee, C.-F.F. A new solution branch for the Blasius equation—A shrinking sheet problem. *Comput. Math. Appl.* **2008**, *56*, 3088–3095. [CrossRef]
21. Fang, T.; Zhang, J. Closed-form exact solutions of MHD viscous flow over a shrinking sheet. *Commun. Nonlinear Sci. Numer. Simul.* **2009**, *14*, 2853–2857. [CrossRef]
22. Fang, T.-G.; Zhang, J.; Yao, S.-S. Viscous flow over an unsteady shrinking sheet with mass transfer. *Chin. Phys. Lett.* **2009**, *26*, 014703. [CrossRef]
23. Fang, T.; Zhang, J. Thermal boundary layers over a shrinking sheet: An analytical solution. *Acta Mech.* **2010**, *209*, 325–343. [CrossRef]
24. Fang, T.; Yao, S.; Zhang, J.; Aziz, A. Viscous flow over a shrinking sheet with a second order slip flow model. *Commun. Nonlinear Sci. Numer. Simul.* **2010**, *15*, 1831–1842. [CrossRef]
25. Sajid, M.; Javed, T.; Hayat, T. MHD rotating flow of a viscous fluid over a shrinking surface. *Nonlinear Dyn.* **2008**, *51*, 259–265. [CrossRef]
26. Yacob, N.A.; Ishak, A. Micropolar fluid flow over a shrinking sheet. *Meccanica* **2012**, *47*, 293–299. [CrossRef]
27. Turkyilmazoglu, M. Mixed convection flow of magnetohydrodynamic micropolar fluid due to a porous heated/cooled deformable plate: Exact solutions. *Int. J. Heat Mass Transf.* **2017**, *106*, 127–134. [CrossRef]
28. Nield, D.A.; Kuznetsov, A.V. The Cheng-Minkowycz problem for natural convective boundary-layer flow in a porous medium saturated by a nanofluid. *Int. J. Heat Mass Transf.* **2009**, *52*, 5796–5801. [CrossRef]
29. Ali, F.M.; Nazar, R.; Arifin, N.M.; Pop, I. Unsteady flow and heat transfer past an axisymmetric permeable shrinking sheet with radiation effect. *Int. J. Numer. Methods Fluids* **2011**, *67*, 1310–1320. [CrossRef]
30. Bhattacharyya, K.; Layek, G.C. Effects of suction/blowing on steady boundary layer stagnation-point flow and heat transfer towards a shrinking sheet with thermal radiation. *Int. J. Heat Mass Transf.* **2011**, *54*, 302–307. [CrossRef]
31. Bhattacharyya, K.; Mukhopadhyay, S.; Layek, G.C.; Pop, I. Effects of thermal radiation on micropolar fluid flow and heat transfer over a porous shrinking sheet. *Int. J. Heat Mass Transf.* **2012**, *55*, 2945–2952. [CrossRef]
32. Dash, G.C.; Tripathy, R.S.; Rashidi, M.M.; Mishra, S.R. Numerical approach to boundary layer stagnation-point flow past a stretching/shrinking sheet. *J. Mol. Liq.* **2016**, *221*, 860–866. [CrossRef]
33. Mishra, S.R.; Khan, I.; Al-mdallal, Q.M.; Asifa, T. Free convective micropolar fluid flow and heat transfer over a shrinking sheet with heat source. *Case Stud. Therm. Eng.* **2018**, *11*, 113–119. [CrossRef]
34. Bejan, A. *Convection Heat Transfer*, 4th ed.; Wiley: Hoboken, NJ, USA, 2013.
35. Mansur, S.; Ishak, A.; Pop, I. Flow and heat transfer of nanofluid past Stretching/shrinking sheet with partial slip boundary conditions. *Appl. Math. Mech.-Engl. Ed.* **2014**, *35*, 1401–1410. [CrossRef]
36. Baranovskii, E.S. Optimal Control for steady flows of the Jeffreys Fluids with slip boundary condition. *J. Appl. Ind. Math.* **2014**, *8*, 168–176. [CrossRef]
37. Dero, S.; Rohni, A.M.; Saaban, A. MHD micropolar nanofluid flow over an exponentially stretching/shrinking surface: Triple solutions. *J. Adv. Res. Fluid Mech. Therm. Sci.* **2019**, *56*, 165–174.
38. Bhat, A.; Katagi, N.N. Magnetohydrodynamic flow of micropolar fluid and heat transfer between a porous and a non-porous disk. *J. Adv. Res. Fluid Mech. Therm. Sci.* **2020**, *75*, 59–78. [CrossRef]
39. Guedri, K.; Mahmood, Z.; Fadhl, B.M.; Makhdoum, B.M.; Eldin, S.M.; Khan, U. Mathematical analysis of nonlinear thermal radiation and nanoparticle aggregation on unsteady MHD flow of micropolar nanofluid over shrinking sheet. *Heliyon* **2023**, *9*, e14248. [CrossRef]
40. Choi, C.K. Slip flow past a solid sphere in a viscous fluid. *J. Fluid Mech.* **1991**, *227*, 113–127.
41. Liao, S. *Homotopy Analysis Method in Nonlinear Differential Equations*; Springer: Berlin/Heidelberg, Germany, 2012.

Disclaimer/Publisher's Note: The statements, opinions and data contained in all publications are solely those of the individual author(s) and contributor(s) and not of MDPI and/or the editor(s). MDPI and/or the editor(s) disclaim responsibility for any injury to people or property resulting from any ideas, methods, instructions or products referred to in the content.